A Precise Calibration Method for Line Scan Cameras

Guoqin Yuan, Lina Zheng, Yalin Ding, Hongwen Zhang, Xuefei Zhang, Xueji Liu, and Jianjun Sun

***Abstract*— With the advantages of ultrahigh resolution and acquisition rate, line scan cameras are increasingly being deployed for precision measurement. In order to achieve high precision, the intrinsic parameters must be calibrated properly. However, the existing calibration models that only calibrate the principle points and the distortion in 1-D direction and ignore the other directions result in limited adaptability and accuracy, which are especially serious for multiline cameras. To conquer this challenge, this article proposes a precise calibration method that is qualified for both multiline cameras and single-line cameras. Through the analysis of the relative position relationship between the pixel array and principle point, a method for calibrating the principle points and the distortion in 2-D direction is proposed and a flexible calibration device is designed based on a theodolite. The calibration quality is improved by the novel calibration method that effectively establishes the correspondence relationship between the rays and pixels by recording the incident angle of the collimated beam and its image, respectively. Moreover, a robust optimization algorithm is proposed to enhance the stability of parameter estimation. The proposed method is verified by Monte-Carlo simulation, real experimental data, and flight. The results show that the 2-D calibration model can improve the calibration accuracy of the multiline cameras by 45 pixels at most, and its reprojection measurement uncertainty is as low as 0.1 pixels. The comparative results of the experiments demonstrate that the proposed method has the advantages of high accuracy, low cost, and easy implementation.**

***Index Terms*— Bidirection distortion, collimated beam, line scan camera, multimodal sensors, sensor calibration.**

I. Introduction

THE line scan cameras are more and more favored in the accurate 3-D surface measurements [1]–[3], such as vehicle-borne 3-D scene reconstruction and space-borne photogrammetric areas [4], thanks to their high resolution, accuracy, and acquisition rate (up to 327368 pixels at 10 kHz) [5].

There are two classes of line cameras: single-line cameras and multiline cameras [6]. The single-line scan camera is a particular matrix camera that consists of only one linear array. The multiline camera has multiple parallel sensor lines, typically with three panchromatic lines and additional multispectral lines in the focal plane of a single lens system.

The multiline cameras have prominent advantages in 3-D image acquisition and high-precision coordinate measurement and 3-D data products such as digital elevation model (DEM), digital orthophoto map (DOM), and digital line graphic (DLG) with small size, lightweight, and high accuracy. In addition, the multiline technique combines photogrammetry and remote sensing which enables new approaches of 3-D scene visualization and reconstruction as well as new applications in airborne and close-range photogrammetry [7]–[10].

The line scan cameras need to be calibrated to extract metric information from the image [11] and [12]. Conventional calibration methods for matrix cameras [13]–[17] are not applicable to the line scan cameras. For single-line cameras, several calibration methods have been developed in the last decades. In detail, there are static calibration and scanning calibration.

The static calibration utilizes patterns on the target consisting of several feature lines. The intersection points of the camera's viewing plane with the feature lines are used for calibration. Horaud [18] applied cross-ratio invariance to calculate the coordinates of these intersection points. The method is easy to implement, however, the calibration target had to accurately translate along the Y- or Z-axis with known increments and the accuracy of displacement will have significant impacts on calibration accuracy. To overcome this limitation, the stereo targets are employed. Luna *et al.* [19] estimate the calibration parameters using a 3-D pattern with multiple planes and a single capture without the precise translation. This method is easier and more flexible to implement, but requires high-precision 3-D targets. Limited by the size of the calibration targets, this method is restricted to scan space points and small calibration volume, which affects the accuracy and stability of the calibration results. However, a large stereo target is costly and not user-friendly. Therefore, static calibration still cannot fulfill the demands of calibration, especially when the camera has a long focal length and a large field of view (FOV).

Scanning calibration estimates the calibration parameters by a series of matrix operations. Drareni proposed a scanning camera calibration method using a planar grid pattern [20]. The pattern moves with a constant velocity relative to the camera and the camera scans the target at an appropriate line rate, and then the scanned 2-D image is obtained. This method can quickly establish the correspondence relationship between the image points and the points on the pattern calibration

Manuscript received February 23, 2021; revised May 19, 2021; accepted May 31, 2021. Date of publication July 27, 2021; date of current version August 4, 2021. This work was supported in part by the National Science and Technology Major Project of China under Grant 30-H32A01-9005-13/15. The Associate Editor coordinating the review process was Yasutaka Amagai. *(Corresponding author: Xuefei Zhang.)*

The authors are with the Key Laboratory of Airborne Optical Imaging and Measurement, Changchun Institute of Optics, Fine Mechanics and Physics, Chinese Academy of Science, Changchun 130033, China (e-mail: yuanguoqin@139.com; ailsazheng@163.com; dingyl1964@sohu.com; zhang_hong_wen@sina.com; zhangxuefei@ciomp.ac.cn; lxj3115@163.com; jianjun_sun@163.com).

Digital Object Identifier 10.1109/TIM.2021.3090157

objects by a linear and efficient scheme. The synchronization between the line rate of the camera and the speed of the target's motion is difficult to achieve. Li *et al.* [21] and Bingwei *et al.* [22], [23] simplified the experimental operation by using 3-D target instead of planar patterns and the algorithms were modified using the velocity in three directions. Scanning calibration provides more points and higher accuracy compared with static calibration. However, it cannot be used in real practice because it requires a pure linear motion under the actual calibration conditions which is not reproducible owing to vibrations and other restrictions.

In general, the traditional calibration models for line scan cameras consider that the lens distortions only exist along the pixel array direction, and ignore distortions in the other direction due to the small distance from the pixel array to the principle point [24]–[26]. For the multiline cameras, there are significant drawbacks to the classical calibration model. The multiline cameras are equipped with multiple lines, some of which have a large distance from the principle point. The distortion is bidirectional and each sensor line is curved which introduces more difficulties on the calibration. Therefore, the traditional calibration methods are no longer suitable to get calibration with high accuracy. In this article, we provide a 2-D and high-precision calibration method for multiline cameras, which can also further improve the precision of single-line cameras calibration due to the fact that the sensor line cannot be guaranteed to accurately fit on the principle point. A novel calibration device is designed based on a theodolite. The calibration quality is improved by the novel calibration method which effectively establishes the correspondence relationship between the rays and pixels by recording the incident angle of the collimated beam and its image, respectively. Meanwhile, the method uses collimated beam for calibration, which provides great convenience for data acquisition and data processing since it gives an image invariant against translation [27]. These characteristics would facilitate the experiment in the actual measurement field. A robust optimization algorithm is also proposed in this article to enhance the stability of parameter estimation. The method works without making a pattern or other calibration targets and has the advantage of more space points, high precision, and efficiency.

The rest of this article is organized as follows. The line scan imaging model is given in Section II. The proposed calibration method is described in Section III. Results from validating the method both in simulation and on real data are presented in Section IV. Finally, Section V presents the conclusions and highlights.

II. Line Scan Imaging Model

The line scan camera can only see the objects in the viewing plane which is defined by the projection center and the pixel array [28]. Fig. 1 is the schematic of the imaging relationship of perspective projection.

Neglecting the lens distortion, the collinearity equation of a space point P $[X\ Y\ Z\ 1]$ in the world frame and the corresponding pixel coordinates $[u\ v\ 1]$ in the image, the line

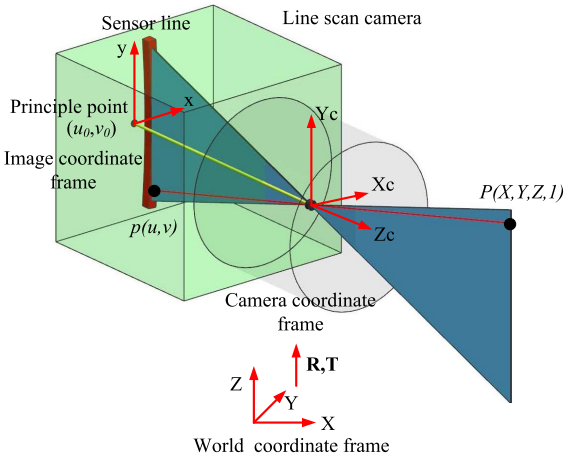

Fig. 1. Image relationship of perspective projection.

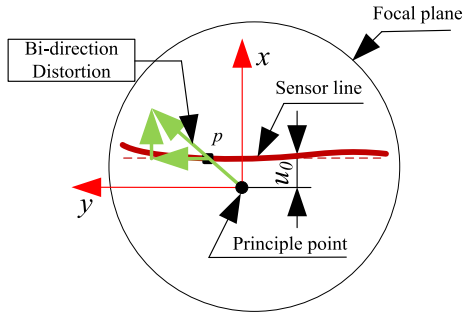

Fig. 2. Distortion model of line scan cameras, axis-y is along the pixel array direction.

scan camera model is demonstrated as below [29]

$$s\begin{bmatrix} u \\ v \\ 1 \end{bmatrix} = \begin{bmatrix} f & 0 & u_0 \\ 0 & f & v_0 \\ 0 & 0 & 1 \end{bmatrix} \begin{bmatrix} R & T \end{bmatrix} \begin{bmatrix} X \\ Y \\ Z \\ 1 \end{bmatrix} \tag{1}$$

where s is an arbitrary scale factor, [**R** **T**] is the extrinsic matrix, specifically, **R** is the rotation matrix and **T** is the translation matrix specifying the relative pose between the world coordinate frame and the camera coordinate frame. f is the principle distance in pixels, and u_0 and v_0 are the coordinates of the principal point on the image, respectively.

The traditional calibration model considers $u_0 = 0$, which is only applicable to the situation that the sensor line accurately installs on the principle point. Due to requiring an extremely complex bundle adjustment, this situation is almost impossible to happen. The general situation is shown in Figs. 1 and 2. The distance between the sensor line and the principle point is u_0 and the distortion exists in two directions.

The multiline cameras are equipped with multiple parallel sensor lines, as shown in Fig. 3. The nadir line is mounted close to the principle point but cannot be guaranteed to accurately fit on the principle point of the lens because of the assembly error. The remaining lines have a larger distance from the principle point. This will lead to a 2-D distortion as shown in Fig. 4, and the 2-D distortion will become more serious as the FOV increases.

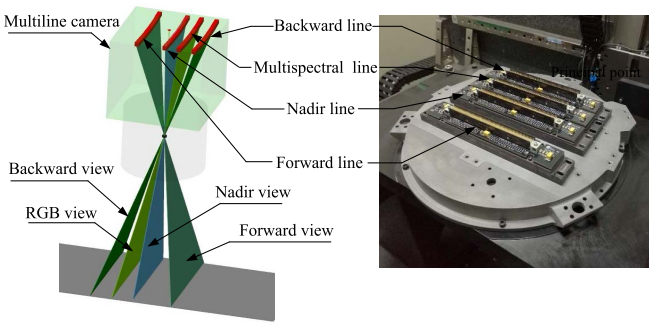

Fig. 3. Structure of a multiline camera.

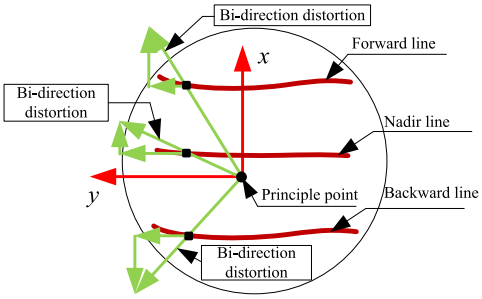

Fig. 4. Multiline camera's distortion characteristics.

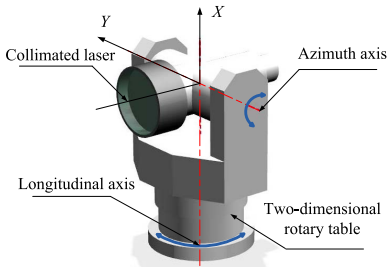

Fig. 5. Structural diagram of the theodolite.

Therefore, whether for multiline cameras or single-line cameras, the traditional method only calibrates one direction principle point and distortion, resulting in reducing the calibration accuracy. So the purpose of calibrating the line scan camera is to estimate the camera intrinsic parameters, including u_0, v_0, f, and distortion in two directions.

III. Calibration Method

A. Calibration Device

Based on the 2-D distortion and imaging model of the line scan camera, we propose a calibration device as shown in Fig. 5. We report for the first time, to the best of our knowledge, the use of theodolite to calibrate the line scan camera. A theodolite consists of a 2-D rotary table named azimuth axis and longitudinal axis. Generally, theodolites also have a collimated laser when used for a laser distance meter [30].

When calibrating the line scan cameras using collimated beam emitted by the theodolites, the image on the sensor is a collimated beam pattern, so each projected image point

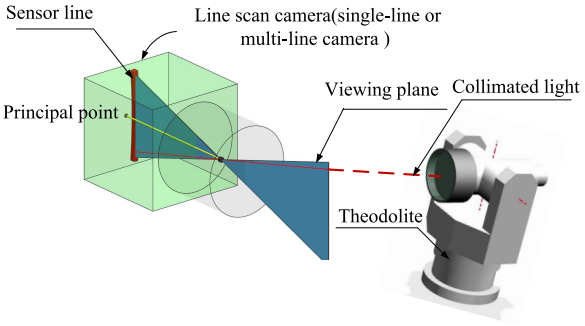

Fig. 6. Imaging features of line-scan camera and schematic of the calibration device.

represents a point at infinity, denoted in 3-D projective space by the homogeneous coordinate P = [X, Y, Z, 0] [31]. Substitute to (1), the obtained mapping of ideal points at infinity is invariant against translation. Comparing to the classical calibration grids method, the relative position of theodolite and camera does not affect the calibration result and less fitting parameters are used.

Fig. 6 illustrates a distorted viewing plane formed by the line sensor and projection center. The two orthogonal axes of the theodolite are adjusted so that the collimated beam is imaged on the sensor line. The imaged coordinate and incidence angles of the collimated beam are recorded, respectively. Repeat the above process to acquire multiple sets of data. The calibration algorithm described in Section III. Part *C*. is applied to finalize the calibration.

B. Data Acquisition

The data acquisition process is shown in Fig. 6. Taking point G_1 as an example, the data acquisition process is described in detail. First, we adjust the theodolite, when the collimated beam image itself on the geometric center(M) of the sensor line, record the azimuth angle of the theodolite and set the longitudinal angle to zero. Then, adjust the longitudinal axis of the theodolite to α_1, as shown in Fig. 6, the collimated beam is imaged at H, failing to image itself on the sensor line, so adjust azimuth angle until the collimated beam can be imaged at G_1, whose coordinate is marked as G_{1x}. Repeat the process, get G_2, G_3,..., G_n at $(\alpha_2, \beta + d\beta_2)$, $(\alpha_3, \beta + d\beta_3)$, ..., $(\alpha_n, \beta + d\beta_n)$. The coordinate of G_2, G_3,..., G_n is marked as G_{2x}, G_{3x},..., G_{nx}.

C. Estimating the Parameters

For the convenience of data processing, image coordinate frame (ICF) xOy and theodolite coordinate frame (TCF) XOY are constructed, respectively. The origin of ICF and TCF is located at the principle point of the lens. The y-axis is the direction of the sensor line. The right-hand coordinate system determines the x-axis. The X-axis is parallel to the theodolite longitudinal axis. The Y-axis is parallel to the azimuth axis of the theodolite. As shown in Fig. 7, the N is the projection of the principle point onto the sensor line. The coordinates of N in ICF are x_0, y_0.

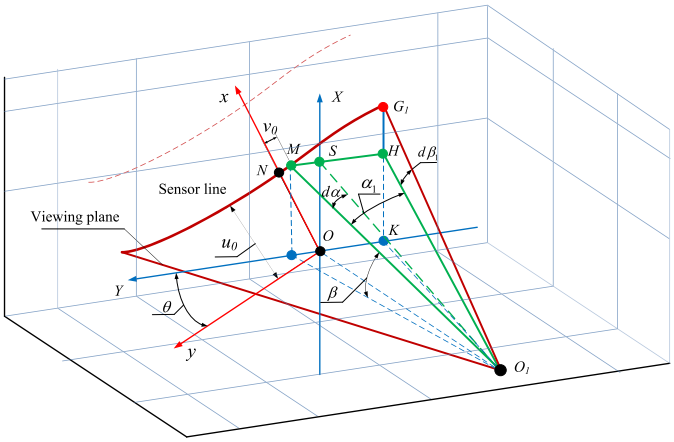

Fig. 7. Geometric schematic of the proposed calibration method.

As shown in Fig. 7, ICF and TCF conversion relationship are as follows:

$$M_{\mathrm{I}} = C_{\mathrm{I}}^{\mathrm{T}} M_{\mathrm{T}}. \tag{2}$$

M_I and M_T are coordinates of M in ICF and TCF, respectively. $C_{\mathrm{I}}^{\mathrm{T}}$ is the 2×2 rotation matrix transforming ICF to TCF

$$C_{\mathrm{I}}^{\mathrm{T}} = \begin{bmatrix} \cos\theta & \sin\theta \\ -\sin\theta & \cos\theta \end{bmatrix} \tag{3}$$

where θ is the angle of the ICF relative to the TCF which can be derived from the proposed method. Therefore, it is not necessary to accurately adjust the mutual positional relationship between the line scan camera and the theodolite before calibration.

In TCF, when the collimated beam rotates around the azimuth axis by α_1, the image moves from point M to point H. According to the geometric relationship in $Rt\Delta OO_1S$, we have

$$\begin{cases} d\alpha = a\tan\left(\dfrac{M_{ox}}{\sqrt{f^2 + M_{Oy}^2}}\right) \\ SO_1 = \sqrt{f^2 + My^2} \end{cases} \tag{4}$$

where f is the principle distance of the camera to be calibrated.

From Fig. 7, we can get

$$\begin{cases} MH \perp Y \\ MH \perp OO_1. \end{cases} \tag{5}$$

So $MH \perp OS$, in $Rt\Delta O_1SH$, we have

$$\begin{cases} SH = \sqrt{f^2 + My^2} \times \tan(\alpha_1 - d\alpha) \\ H_{0\ x} = M_{0\ x} + SH \\ H_{Oy} = M_{Oy}. \end{cases} \tag{6}$$

In $Rt\Delta OKO_1$, $Rt\Delta G_1KO_1$, we have

$$\begin{cases} O_1K = \sqrt{f^2 + SH^2} \\ G_{10\ y} = O_1K \times \tan(\beta + d\beta_1) \\ G_{10\ x} = H_{Ox} \end{cases} \tag{7}$$

where $G_{10\ x}$, $G_{10\ y}$ are the coordinates of G_1 in ICF. From (3) we can get

$$G_{N1} = (C_N^O)^{-1}(G_{O1}). \tag{8}$$

$G_{N1}(G_{N1x}, G_{N1y})$ is the ideal coordinate according to the pinhole model with incident angle $(\alpha_1, \beta + d\beta_1, \theta)$, whose actual coordinate is $G_{1x}, 0$. The difference is the distortion. The distortion of G_1 is

$$\begin{cases} DG_{1\ x} = G_{1\ x} - G_{N1\ x} \\ DG_{1\ y} = -G_{N1\ y}. \end{cases} \tag{9}$$

In the same way, the distortion of G_1, G_2, G_3,..., G_n can be obtained. The maximum likelihood estimate can be obtained by minimizing the following functional:

$$\sum_{i=1}^{n} ||G_{\mathrm{N}ix} - \hat{G}(u_0, v_0, f, \theta, \alpha_i, \beta + d\beta_i)||^2 \tag{10}$$

where $\hat{G}(u_0, v_0, f, \theta, \alpha_i, \beta + d\beta_i)$ is the ideal image point coordinate from (11) when the two axes of the theodolite are $\alpha_i, \beta + d\beta_i$. The solution of (11) is a nonlinear optimization problem, which is solved with the Levenberg–Marquardt algorithm as implemented in Minpack [32]. It requires an initial guess of x_0, y_0, f, θ, which can be obtained using the design value.

Equation (11) can also be solved according to the physical meaning of distortion. u_0, v_0, and f satisfy $\min\left(\sum_{i=1}^{n}\left(DG_{ix}{}^2 + DG_{iy}{}^2\right)\right)$, we have

$$\begin{cases} \dfrac{\partial \sum_{i=1}^{n}\left(DG_{ix}{}^2 + DG_{iy}{}^2\right)}{\partial x_0} = 0 \\ \dfrac{\partial \sum_{i=1}^{n}\left(DG_{ix}{}^2 + DG_{iy}{}^2\right)}{\partial y_0} = 0 \\ \dfrac{\partial \sum_{i=1}^{n}\left(DG_{ix}{}^2 + DG_{iy}{}^2\right)}{\partial f} = 0 \end{cases} \tag{11}$$

Equation (12) has variables u_0, v_0, f, and θ. At each sampling point, there are three equations. When $3\ n \geq 5$, we can solve u_0, v_0, f, and θ.

Substitute u_0, v_0, f, and θ to (10), we have the distortion value of G_1, G_2, G_3,..., G_n in two directions. In principle, this method can calibrate the distortion of all the pixels and avoid establishing a distortion model of a large FOV lens. In addition, this method is qualified for both multiline cameras and single-line cameras. When calibrating multiline cameras, the above process can be repeated on each line, respectively.

IV. Validation

The simulation analysis was carried out in Section IV. Part *A*. The multiline camera was calibrated in the laboratory in Section IV. Part *B*. The effectiveness of the proposed method was verified by the flight test in Section IV. Part *C*.

A. Simulation

The parameters of the simulation are summarized in Table I which are similar to those used in [29]. The theodolite is

TABLE I
SPECIFICATIONS OF CALIBRATION SETUP AND CAMERA

Parameters	Values	mean
f	25mm	Ground truth value of the principle length
sensor's length in pixel	2048	Number of pixels of the sensor line
u_0	0-0.5mm	Ground truth value of the principle point
v_0	0.25mm	Ground truth value of the principle point
Pixel dimension	5μm	pixel size
Least square optimiser	Levenberg–Marquardt	Algorithm for solving Eq.(11)

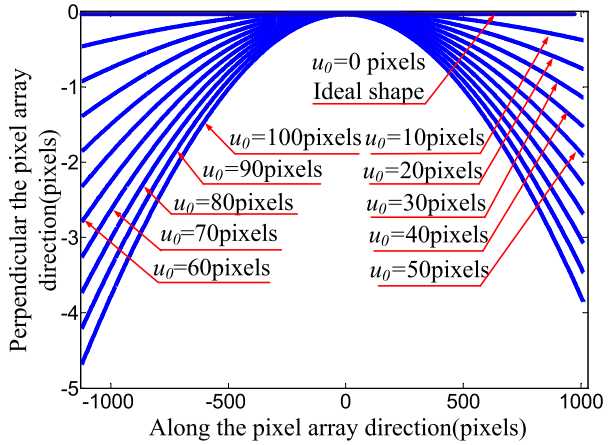

Fig. 8. Actual shape of the line sensor on the focal plane as a function of v_0 (v_0 =50 pixels, u_0 = 0–100 pixels.

placed directly in front of the line camera. The calibration target is not needed.

Different from the classical calibration method, our method considers the distance between the sensor line and the principle point. According to Table I, the actual shape of the sensor line in the focal plane is affected by the distortion in two directions, as shown in Fig. 8.

As can be seen from Fig. 8, the distortion perpendicular to the sensor line increases as the distance between the pixels array and principle point increases. When the distance is 10 pixels (that is 0.05 mm), the distortion is 1 pixel. When the distance is 100 pixels (that is 0.5 mm, which is a small distance that may cause by assembling error), the maximum distortion perpendicular to the sensor line direction is up to 5 pixels. Therefore, it is necessary to consider the bidirectional distortion of the sensor line in precision calibration.

In the simulation, adjust the two orthogonal axes of the theodolite, and place the collimated beam in the viewing plane of the line scan camera. Fig. 9 shows the simulation results of the azimuth and altitude angles of theodolite according to the steps described in Section III. Part *C*. It is obtained by labeling each pixel to avoid establishing the distortion model, adjusting the two orthogonal axes of the theodolite, and placing the collimated beam in the viewing plane of the line scan camera.

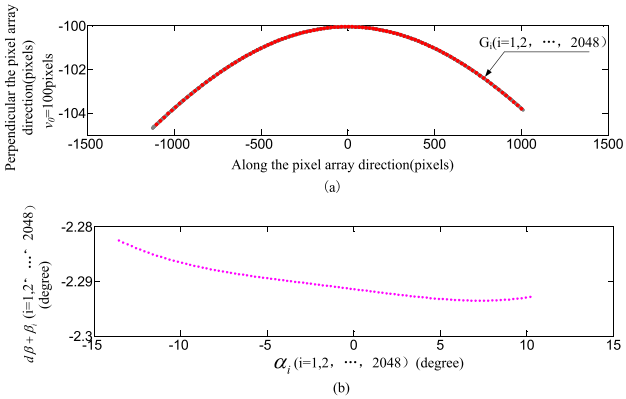

Fig. 9. Simulation. (a) Labeled pixels G_i, (i = 1,2,…, 2048). (b) Calculated azimuth and longitudinal angles of G_i.

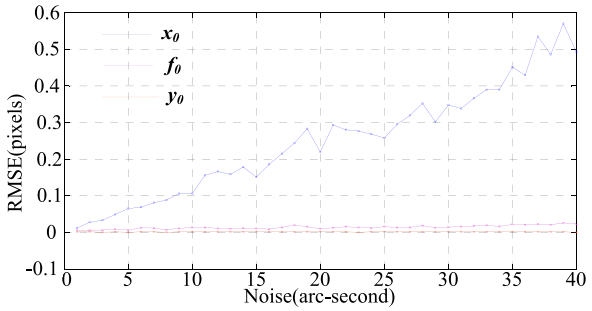

Fig. 10. RMSE in camera intrinsic parameters versus azimuth axis noise.

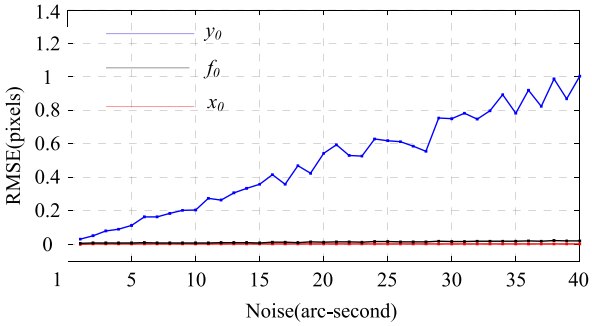

Fig. 11. RMSE in camera intrinsic parameters versus longitudinal axis noise.

Here, two simulated experiments are performed. Part *1* examines the effects of azimuth axis noise on the estimated intrinsic parameters. Part *2* models the effect of a longitudinal axis noise on the estimated intrinsic parameters.

1) Effect of Azimuth Axis Noise on Calibration Result: The effect of azimuth axis noise on calibration result is tested by gradually adding the levels of Gaussian noise, ranging from 1 to 40 arc-second. For each noise level, we perform 200 independent trials. The root-mean-square error (RMSE) in the intrinsic parameter estimates are shown in Fig. 10.

It can be observed in Fig. 10 that the calibration error increases as the azimuth axis noise increases. The azimuth axis noise has a great influence on the accuracy of x_0. When the azimuth axis noise of the theodolite is 10 arc seconds, the x_0 calibration accuracy is about 0.1 pixels.

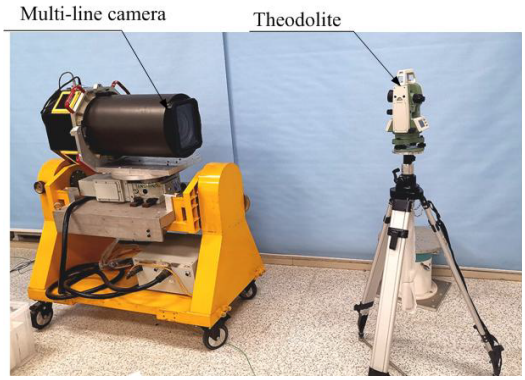

Fig. 12. Photograph of the line scan camera 2-D calibration in lab.

2) Influence of Longitudinal Axis Noise on Calibration Result: We vary the noise level from 1 pixel to 40 pixels. For each noise level, we perform 200 independent trials. The results are shown in Fig. 11. The calibration error increases when the longitudinal axis noise increases. The longitudinal axis noise has a great influence on the accuracy of y_0. When the longitudinal axis noise of the theodolite is 10 arc seconds, the calibration accuracy of y_0 is about 0.2 pixels.

B. Experimental Results

The laboratory calibration device is shown in Fig. 12. The camera (Changchun Institute of Optics, Fine Mechanics and Physics, Chinese Academy of Sciences (CIOMP) digital measurement system (AMS)-3000) has three panchromatic lines on the focal plane. The resolution of each sensor line is 32 756. The pixel size is 5 μm and the focal length is 130 mm. The theodolite has been precisely calibrated and inspected before use. The measurement uncertainty of altitude and longitudinal angle is 2 arc seconds. Since the mapping of the collimated beam is invariant against translation [33], the distance between the camera and the theodolite does not affect the calibration. However, we need to put the theodolite at a suitable distance to obtain a suitable brightness image and to ensure that the collimated beam can be imaged on all pixels of the sensor line only by adjusting the 2-D rotary table.

In order to extract an accurate point coordinate, the image is recorded at a camera line rate of 1040 Hz. A total of 200 lines for each image are acquired. The image point center of each line is collected as image point coordinates.

In brief, the procedure can be summarized by the following steps.

Step 1: Place the theodolite at a suitable position relative to the camera to obtain an appropriate bright image and ensure that the collimated beam can be imaged on all pixels by adjusting the 2-D rotary table.

Step 2: Adjust the theodolite, when the collimated beam image itself on the geometric center (M) of the sensor line, record the azimuth angle of the theodolite. and set the longitudinal angle to zero.

Step 3: Adjust the theodolite until the collimated beam can be imaged at the next pixel, record the value of longitudinal angle and azimuth angle.

Step 4: Repeat the process.

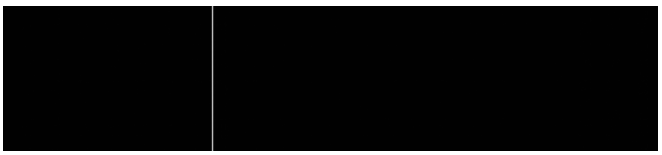

Fig. 13. Image captured by the line scan camera.

One of the acquired images is shown in Fig. 13. Positions of the image were extracted from the line-scan images by grayscale extraction algorithm with subpixel precision [34].

Finally, according to the pixel coordinates of all the calibration pixels and the corresponding longitudinal and azimuth angles, the calibration parameters are solved according to (11). The total data acquisition process costs about 5 h.

The calibration results are shown in Fig. 14.

It can be found from Fig. 14 that there is significant distortion in two directions. The maximum distortion of the perpendicular sensor line direction is almost 45 pixels in the backward line and 43 pixels in the forward line. Even the precise-assembled nadir line has almost 8 pixels due to assembly errors. This is obviously not to be overlooked.

Two conclusions can be drawn through the experiment:

1) For both single-line and multiline cameras, in general, the sensor line deviates from the principle point of the lens, and the line scan camera has distortion in two directions. Both simulation (Fig. 8) and experimental (Fig. 14) results show that the proposed method improves the calibration accuracy compared with the traditional calibration of only one direction.

2) The proposed method only needs to use a theodolite to complete the calibration, has no dependence on making a calibration board. The proposed method can get more calibration point data, calibrate each pixel of the linear array, and avoid the error of establishing a distortion model of the optical system with a large FOV.

In order to verify the accuracy of the proposed method, a verification experiment is carried out, as shown in Part C.

C. Verification Experiment

In order to verify calibration accuracy, we chose an area of 64 km^2 to make a flight verification experiment. The procedure is briefly described as follows. First, there are 278 precision-measured 3-D checkpoints placed on the ground. Then, the camera is loaded on the aircraft and takes pictures of the checkpoints to obtain actual images. Third, taking the measured 3-D checkpoints projected in the cameras with the camera calibration parameters again, obtaining reprojected points in the camera. Lastly, calculate the pixel value between the actual points and the reprojected ones. The evaluation criteria are the reprojection error between the actual point and the calculated projection point.

Fig. 15 shows a photograph of the camera in the aircraft. The checkpoint distribution and the camera flight path are shown in Fig. 16. One of the acquired images is shown in Fig. 17.

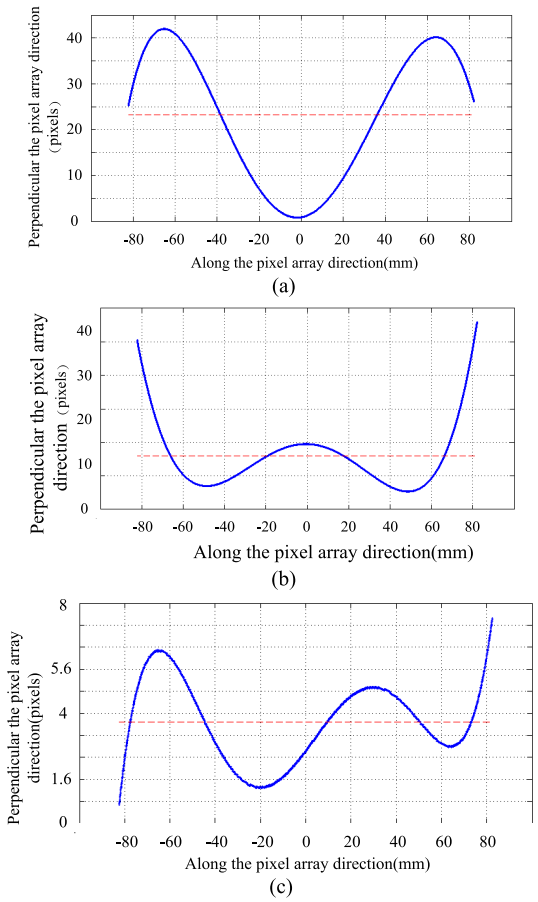

Fig. 14. Shape of multiple lines due to the 2-D distortion. (a) Shape of the forward line. (b)The shape of the backward line. (c) Shape of the nadir line.

Fig. 15. Photograph of the camera in the aircraft.

The reprojection error is shown in Fig. 18, according to which we can get the measurement uncertainty δ_e

$$\delta_e = \frac{1}{n-1}\sqrt{\sum_{i=1}^{n}(e_{ai}^2 + e_{pi}^2)} \tag{12}$$

where, e_{ai} and e_{pi} are the reprojection error along the pixels array and perpendicular to the pixels array. n is the number of checkpoints, $n = 278$. From (12) and Fig. 18, we can get the measurement uncertainty as 0.1 pixels and the maximum error is 0.38 pixels. Due to 2-D calibration, the proposed method has the same precision in two directions, perpendicular and

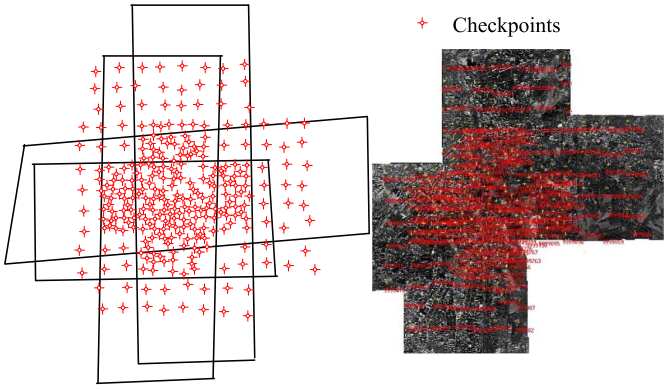

Fig. 16. Flight path and checkpoints distribution.

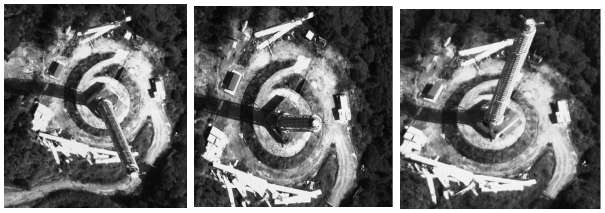

Fig. 17. Image captured by flight verification experiment. (a) Forward-view image. (b) Nadir-view image. (c) Backward-view image.

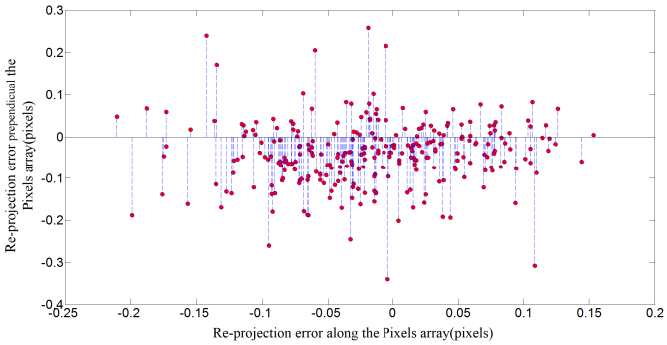

Fig. 18. Reprojection error.

along the pixels array. Compared with the traditional method of calibrating only one direction, our method is significantly improved. As shown in Fig. 14, our method improves the calibration accuracy of the multiline cameras by 45 pixels at most. All the above results indicate that the flight experiments prove the correctness of the method.

V. Conclusion

This article proposes a static, 2-D, high-precision calibration method that is qualified for both multiline cameras and single-line cameras. The method further improves the calibration precision of line scan cameras whose accuracy is usually degraded by the fact that the sensor lines cannot be accurately fitted on the principle point of the lens. Another contribution of this article is the design and implementation of a calibration device for line scan cameras. Specifically, the proposed method can calibrate the principle point and

distortion in 2-D directions. Using the infinity target as the calibration object, the correspondence relationship between the calibration object and the image point coordinates can be effectively established, and the calibration process is efficient. Therefore, there is no need to make a calibration target manually. Comprehensive simulation and experimental results show our proposed method is able to obtain more accurate and consistent results compared to previous methods. As shown in Fig. 14, the proposed method improves the calibration accuracy of the backward line, the forward line, and the nadir line by 45 pixels, 43 pixels, and 8 pixels, respectively. Therefore, our method could handle errors effectively and can achieve excellent calibration accuracy with the reprojection error as low as 0.1 pixels.

In practice, it is necessary to adjust the two orthogonal axes of the theodolite when imaging the collimated beam of the theodolite at each calibration pixel, which may consume lots of working time. In near future, the aim is to design an automatic calibration device with the capability of theodolite shaft adjustment and linear scan camera imaging to further reduce the calibration time.

REFERENCES

[1] E. Lilienblum and A. Al-Hamadi, "A structured light approach for 3-D surface reconstruction with a stereo line-scan system," *IEEE Trans. Instrum. Meas.*, vol. 64, no. 5, pp. 1258–1266, May 2015.

[2] B. Sun, J. Zhu, L. Yang, S. Yang, and Y. Guo, "Sensor for in-motion continuous 3D shape measurement based on dual line-scan cameras," *Sensors*, vol. 16, no. 11, p. 1949, Nov. 2016.

[3] Y. Pi, X. Li, and B. Yang, "Global iterative geometric calibration of a linear optical satellite based on sparse GCPs," *IEEE Trans. Geosci. Remote Sens.*, vol. 58, no. 1, pp. 436–446, Jan. 2020.

[4] B. Sun, J. Zhu, L. Yang, S. Yang, and Y. Guo, "Sensor for in-motion continuous 3D shape measurement based on dual line-scan camera," *Sensors*, vol. 16, no. 11, p. 1949, Nov. 2016.

[5] L. Zheng *et al.*, "Efficient acquisition of geographic big data: Domestic three-line stereo aerial photography system," in *China's e-Science Blue Book 2018*. Singapore: Springer, Jan. 2020, pp. 205–218.

[6] R. Reulke, S. Becker, N. Haala, and U. Tempelmann, "Determination and improvement of spatial resolution of the CCD-line-scanner system ADS40," *ISPRS J. Photogramm. Remote Sens.*, vol. 60, no. 2, pp. 81–90, Apr. 2006.

[7] R. Sandau *et al.*, "Design principles of the LH systems ADS40 airborne digital sensor," in in *Proc. Int. Arch. Photogramm. Remote Sens.*, Amsterdam, The Netherlands, Jan. 2000, pp. 258–265.

[8] A. Eckardt and R. Reulke, "Hardware concept of the first commercial airborne digital sensor," in *Proc. SPIE*, vol. 4488. pp. 82–93, Jan. 2002.

[9] Y. Zhang, M. Zheng, J. Xiong, Y. Lu, and X. Xiong, "On-orbit geometric calibration of ZY-3 three-line array imagery with multistrip data sets," *IEEE Trans. Geosci. Remote Sens.*, vol. 52, no. 1, pp. 224–234, Jan. 2014.

[10] B. Emmanuel, Z. Li, and H. Eisenbeiss, "DSM generation and interior orientation determination of IKONOS images using a testfield in Switzerland," *Photogrammetrie-Fernerkundung-Geoinf.*, vol. 2006, no. 1, pp. 41–54, Oct. 2009.

[11] Y. Chen, Z. Xie, Z. Qiu, Q. Zhang, and Z. Hu, "Calibration and validation of ZY-3 optical sensors," *IEEE Trans. Geosci. Remote Sens.*, vol. 53, no. 8, pp. 4616–4626, Aug. 2015.

[12] C. Zhang *et al.*, "First observation of tropospheric nitrogen dioxide from the environmental trace gases monitoring instrument onboard the GaoFen-5 satellite," *Light, Sci. Appl.*, vol. 9, no. 1, pp. 1–9, Apr. 2020.

[13] M. Lee, H. Kim, and J. Paik, "Correction of barrel distortion in fisheye lens images using image-based estimation of distortion parameters," *IEEE Access*, vol. 7, pp. 45723–45733, Apr. 2019.

[14] G. Yuan, L. Zheng, J. Sun, X. Liu, X. Wang, and Z. Zhang, "Practical calibration method for aerial mapping camera based on multiple pinhole collimator," *IEEE Access*, vol. 8, pp. 39725–39733, Dec. 2020.

[15] R. Tsai, "A versatile camera calibration technique for high-accuracy 3D machine vision metrology using off-the-shelf TV cameras and lenses," *IEEE J. Robot. Autom.*, vol. RA-3, no. 4, pp. 323–344, Aug. 1987.

[16] Z. Zhang, "A flexible new technique for camera calibration," *IEEE Trans. Pattern Anal. Mach. Intell.*, vol. 22, no. 11, pp. 1330–1334, Dec. 2000.

[17] L. Zheng, G. Yuan, X. Leng, and Y. Wu, "Calibration method for mapping camera based on a precise grouped approach method," *Int. J. Pattern Recognit. Artif. Intell.*, vol. 32, no. 11, pp. 20241–20248, May 2018.

[18] R. Horaud, R. Mohr, and B. Lorecki, "On single-scanline camera calibration," *IEEE Trans. Robot. Autom.*, vol. 9, no. 1, pp. 71–75, Feb. 1993.

[19] C. A. Luna, M. Mazo, J. L. Lázaro, and J. F. Vazquez, "Calibration of line-scan cameras," *IEEE Trans. Instrum. Meas.*, vol. 59, no. 8, pp. 2185–2190, Aug. 2010.

[20] J. Draréni, S. Roy, and P. Sturm, "Plane-based calibration for linear cameras," *Int. J. Comput. Vis.*, vol. 91, no. 2, pp. 146–156, Jan. 2011.

[21] D. Li, G. Wen, B. Wei Hui, S. Qiu, and W. Wang, "Cross-ratio invariant based line scan camera geometric calibration with static linear data," *Opt. Lasers Eng.*, vol. 62, pp. 119–125, Nov. 2014.

[22] B. Hui, G. Wen, P. Zhang, and D. Li, "A novel line scan camera calibration technique with an auxiliary frame camera," *IEEE Trans. Instrum. Meas.*, vol. 62, no. 9, pp. 2567–2575, Sep. 2013.

[23] B. Hui, J. Zhong, G. Wen, and D. Li, "Determination of line scan camera parameters via the direct linear transformation," *Proc. SPIE*, vol. 51, Nov. 2012, Art. no. 113201.

[24] P. Zhang, T. Takeda, J. A. Toque, Y. Murayama, and A. Ide-Ektessabi, "A line scan camera based stereo method for high resolution 3D image reconstruction," *Proc. SPIE*, vol. 9018, Feb. 2014, Art. no. 901807.

[25] S. Fang, X. Xia, and Y. Xiao, "A calibration method of lens distortion for line scan cameras," *Optik, Int. J. Light Electron Opt.*, vol. 124, no. 24, pp. 6749–6751, Dec. 2013.

[26] R. Liao, J. Zhu, L. Yang, J. Lin, B. Sun, and J. Yang, "Flexible calibration method for line-scan cameras using a stereo target with hollow stripes," *Opt. Lasers Eng.*, vol. 113, pp. 6–13, Feb. 2019.

[27] M. Bauer, D. Grießbach, A. Hermerschmidt, S. Krüger, M. Scheele, and A. Schischmanow, "Geometrical camera calibration with diffractive optical elements," *Opt. Exp.*, vol. 25, no. 25, pp. 20241–20248, 2008.

[28] B. Sun, J. Zhu, L. Yang, S. Yang, and Z. Niu, "Calibration of line-scan cameras for precision measurement," *Appl. Opt.*, vol. 55, no. 25, pp. 6836–6843, Sep. 2016.

[29] D. Su, A. Bender, and S. Sukkarieh, "Improved cross-ratio invariant-based intrinsic calibration of a hyperspectral line-scan camera," *Sensors*, vol. 18, no. 6, p. 1885, Jun. 2018.

[30] X. H. Zhang, "A universal and flexible theodolite-camera system for making accurate measurements over large volumes," *Opt. Laser Eng.*, vol. 50, no. 11, pp. 1611–1620, 2012.

[31] R. C. McPhedran, G. H. Derrick, and L. C. Brown, "Theory of crossed gratings," in *Electromagnetic Theory of Gratings*, R. Petit, Ed. Berlin, Germany: Springer-Verlag, 1980, pp. 227–275.

[32] J. J. Moré, "The Levenberg–Marquardt algorithm, implementation and theory," in *Numerical Analysis* (Lecture Notes in Mathematics), vol. 630, G. A. Watson, Ed. Berlin, Germany: Springer-Verlag, 1977.

[33] S. Thibault, A. Arfaoui, and P. Desaulniers, "Cross-diffractive optical elements for wide angle geometric camera calibration," *Opt. Lett.*, vol. 36, no. 24, pp. 4770–4772, Dec. 2011.

[34] B. F. Alexander and K. C. Ng, "Elimination of systematic error in subpixel accuracy centroid estimation," *Opt. Eng.*, vol. 30, no. 9, pp. 1320–1331, Sep. 1991.

Guoqin Yuan received the M.S. degree from Jilin University, Changchun, China, in 2007, and the Ph.D. degree in optical engineering from the University of the Chinese Academy of Sciences, Beijing, China, in 2012.

He is currently a Researcher with the Changchun Institute of Optics, Fine Mechanics and Physics, Changchun. He is the author of three books, more than 20 articles, and more than 10 inventions. His current research interests include optical imaging and photogrammetry and remote sensing.

Lina Zheng received the B.S. degree in electronics from Jilin University, Changchun, China, in 2003, and the M.S. degree in mechatronics and the Ph.D. degree in optical engineering from the University of the Chinese Academy of Sciences, Beijing, China, in 2008 and 2013, respectively.

She is currently a Researcher with the Changchun Institute of Optics, Fine Mechanics and Physics, Changchun. Her current research interests include optical imaging and mapping techniques for aerial remote camera.

Yalin Ding received the M.S. degree from Northeastern University, Boston, MA, USA, in 1994.

He is currently a Researcher with the Changchun Institute of Optics, Fine Mechanics and Physics, Changchun, China, and also a Supervisor of postgraduate with the University of the Chinese Academy of Sciences, Beijing, China. His current research interest includes optical imaging techniques for aerial remote camera.

Hongwen Zhang received the M.S. degree from the Changchun Institute of Optics, Fine Mechanics and Physics (CIOMP), Changchun, China, in 2003, and the Ph.D. degree in mechatronics engineering from the Changchun University of Science and Technology, Changchun, in 2016.

He is currently a Researcher with CIOMP. His current research interest includes optical imaging techniques for aerial remote camera.

Xuefei Zhang received the M.S. degree from Jilin University, Changchun, China, in 2007, and the Ph.D. degree in optical engineering from the University of the Chinese Academy of Sciences, Beijing, China, in 2012.

She is currently an Associate Researcher with the Changchun Institute of Optics, Fine Mechanics and Physics, Changchun. Her current research interests include automatic match, high-precision geometric processing of remote sensing imagery.

Xueji Liu received the M.S. degree from the National University of Defense Technology, Changsha, China, in 2015.

He is currently a Research Assistant with the Changchun Institute of Optics, Fine Mechanics and Physics, Changchun, China. His current research interests include optical system design and mapping techniques for aerial remote camera.

Jianjun Sun received the M.S. degree from Beihang University, Beijing, China, in 2012.

He is currently a Research Assistant with the Changchun Institute of Optics, Fine Mechanics and Physics, Chinese Academy of Sciences, Changchun. His current research interests include optical imaging and mapping techniques for aerial remote camera.